Photodynamics Simulations of Thymine: Relaxation into the First Excited Singlet State†

Jaroslaw J. Szymczak,*,‡ Mario Barbatti,*,‡ Jason T. Soo Hoo,§ Jaclyn A. Adkins,|| Theresa L. Windus,⊥ Dana Nachtigallová,# and Hans Lischka*,‡,#

Institute for Theoretical Chemistry, University of Vienna, Waehringergrstrasse 17, A 1090 Vienna, Austria, Departments of Physics, Siena College, 515 Loudon Road, Loudonville, New York 12211, Department of Chemistry, Northwest Missouri State University, 800 University Drive, Maryville, Missouri 64468, Department of Chemistry, Iowa State University, 1605 Gilman Hall, Ames, Iowa 50011, and Institute of Organic Chemistry and Biochemistry, Academy of Sciences of the Czech Republic, Flemingovo nam. 2, CZ-16610 Prague 6, Czech Republic

Received: May 30, 2009; Revised Manuscript Received: August 1, 2009

Ab initio nonadiabatic dynamics simulations are reported for thymine with focus on the $S_2 \rightarrow S_1$ deactivation using the state-averaged CASSCF method. Supporting calculations have been performed on vertical excitations, S_1 and S_2 minima, and minima on the crossing seam using the MS-CASPT2, RI-CC2, MR-CIS, and MR-CISD methods. The photodynamical process starts with a fast (<100 fs) planar relaxation from the S_2 $\pi\pi^*$ state into the $\pi_O\pi^*$ minimum of the S_2 state. The calculations demonstrate that two π-excited states (denoted $\pi\pi^*$ and $\pi_O\pi^*$) are actually involved in this stage. The time in reaching the S_2/S_1 intersections, through which thymine can deactivate to S_1, is delayed by both the change in character between the states as well as the flatness of the S_2 surface. This deactivation occurs in an average time of 2.6 ps at the lowest-energy region of the crossing seam. After that, thymine relaxes to the $n\pi^*$ minimum of the S_1 state, where it remains until the transfer to the ground state takes place. The present dynamics simulations show that not only the $\pi_O\pi^*$ S_2 trapping but also the trapping in the $n\pi^*$ S_1 minimum contribute to the elongation of the excited-state lifetime of thymine.

1. Introduction

Upon UV excitation, all five naturally occurring nucleobases return to the ground state on an ultrafast time scale ranging from half a picosecond to a few picoseconds.[1–5] The ultrafast decay minimizes the time that the molecule remains in reactive excited states, which could induce photochemical damage. This enhanced photostability might have been one factor favoring the selection of these bases in early biotic ages, to the detriment of other similar molecules with long-lived excited states.

In general, ultrafast decay depends on the existence of reaction pathways connecting the Franck−Condon region to the seam of conical intersections between the excited and ground states where radiationless processes can occur. For this reason, a great deal of theoretical work has been dedicated to the characterization of reaction paths and conical intersections not only for the five nucleobases[6–18] but also for their isomers,[11,19] substituted species,[12,20,21] and base models.[22,23] Further progress has been achieved by means of dynamics simulations, which attempt to describe the excited-state time evolution and the most frequently accessed reaction pathways. However, balancing the computational costs of dynamics simulations lasting for several picoseconds while still maintaining a proper description of multiple electronic excited states and their nonadiabatic couplings still constitutes a major challenge. Despite the difficulties, semiempirical,[24–26] density functional,[27] and ab initio[28–31] nonadiabatic dynamics simulations have been reported recently for nucleobases.

Among the five nucleobases, thymine has the longest lifetime.[1,2] Femtosecond-resolved pump−probe resonant ionization experiments pumped at 267 nm have revealed two exponential decay components, 6.4 and 100 ps, with the longer one assigned to the triplet-state population.[2] Another set of mass-selected femtosecond-resolved pump−probe resonant ionization experiments also pumped at 267 nm and identified a two-step mechanism with time constants 105 fs and 5.12 ps.[1] In the time-resolved photoelectron spectroscopy experiments reported in ref 4, three time constants were obtained, <50, 490 and 6.4 ps (pump energy at 250 nm). Even though there is no full agreement about the details of the deactivation process, a time constant in the range of 5 to 6 ps for deactivation to the ground state clearly emerges from all of these experimental results. This time constant is, in addition, much larger than those measured for the other nucleobases (adenine: 1.1 ps, cytosine: 1.86 ps, guanine: 0.36 ps, uracil: 1.05 ps[1]).

On the basis of the reaction paths connecting the Franck−Condon region to the S_1/S_0 conical intersections, Perun et al.[13] have proposed that the relatively long lifetime of thymine could be explained by a trapping of the molecule in the dark S_1 $n\pi^*$ state after fast deactivation from the S_2 $\pi\pi^*$ state. Nevertheless, multiple spawning dynamics simulations performed by Hudock et al.[29] at the complete active space self-consistent field (CASSCF) level have found a surprisingly small $S_2 \rightarrow S_1$ deactivation yield in the first half picosecond. These authors then proposed that the reason for the long lifetime is the trapping of thymine in a S_2 minimum right after the photoexcitation. On the basis of the analysis of the reaction paths connecting the minimum in the S_1 state to the S_1/S_0 conical intersections, Zechmann and Barbatti[14] have discussed how the low efficiency of those paths should be an additional factor adding to the S_2 trapping to delay the deactivation to the ground state. Recently

† Part of the "Russell M. Pitzer Festschrift".

* Corresponding authors. E-mail: jaroslaw.szymczak@univie.ac.at (J.J.S.); mario.barbatti@univie.ac.at (M.B.); hans.lischka@univie.ac.at (H.L.).

‡ University of Vienna.

§ Siena College.

|| Northwest Missouri State University.

⊥ Iowa State University.

Academy of Sciences of the Czech Republic.

10.1021/jp905085x CCC: $40.75
Published on Web 08/19/2009

reported nonadiabatic dynamics simulations for thymine at the OM2 semiempirical level[26] did not show S_2 trapping, and the $S_2 \rightarrow S_1$ deactivation was predicted to occur in only 17 fs. The $S_1 \rightarrow S_0$ deactivation took place mainly by means of a reaction path involving the nπ* state and occurred in 420 fs, which is one order of magnitude shorter than the experimental results.

Merchán et al.[32] have proposed a unified model to explain the ultrafast decay of the pyrimidine nucleobases. According to these authors, the deactivation of thymine, uracil, and cytosine can be explained on the basis of the $\pi\pi$* state alone, without any relevant influence of the nπ* state. After the excitation into the $\pi\pi$* state, each of these molecules would either follow a barrierless $\pi\pi$* path to the conical intersection with the ground state or relax into a S_1 $\pi\pi$* minimum before finally moving toward the conical intersection with the ground state. These two paths would give origin to two time constants: one in the femtoseconds time scale related to the direct path and another in the picosecond time scale related to the indirect path.

In summary, three different hypotheses have been proposed to explain the long lifetime of thymine: (1) trapping in the dark S_1 nπ* state,[13] (2) trapping in the S_2 $\pi\pi$* state,[29] and (3) trapping in the S_1 $\pi\pi$* state.[32] In the present work, nonadiabatic dynamics simulations are reported for thymine performed at the CASSCF level propagated for a simulation time of 3 ps, which has been long enough to determine the time constant for the $S_2 \rightarrow S_1$ deactivation process and to examine in detail the mechanistic processes. The dynamics simulations show that the S_2-trapping hypothesis,[29] proposed on the basis of a short time window of 0.5 ps, is fully supported by longer dynamics simulations and that the nπ* state plays an important role in the subsequent steps.

2. Computational Details

Mixed quantum-classical dynamics simulations were performed for thymine at the CASSCF level. The active space was composed of ten electrons in eight orbitals (CASSCF(10,8)). At the ground-state minimum geometry, these are composed of one n, four π, and three π* orbitals. (See Figure S1 in the Supporting Information.) State averaging was performed over three states (SA-3), and the 6-31G*[33] basis set was employed. Analytic energy gradients, nonadiabatic coupling vectors, and minima on the crossing seam were computed by the procedures described in refs 34–38.

We performed mixed quantum-classical dynamics[39] by integrating Newton's equations for the nuclear motion in time steps of 0.5 fs using the Velocity−Verlet algorithm[40] and the time-dependent electronic Schroedinger equation with the fifth-order Butcher algorithm.[41] The partial coupling approximation[42] was used to reduce the number of nonadiabatic coupling vectors computed in each time step. The time-dependent adiabatic populations were corrected for decoherence effects[43] ($\alpha = 0.1$ hartree) and used for computing the surface hopping probabilities for nonadiabatic transitions according to the fewest-switches algorithm[39,44] in the version proposed by Hammes−Schiffer and Tully.[45] Initial geometries and velocities were generated by a Wigner distribution treating each nuclear coordinate as a harmonic oscillator in the ground state. This distribution is characterized by the absorption spectrum in Figure S2 of the Supporting Information. The absorption spectrum was computed by the Gaussian broadening method described in ref 46. Seventy trajectories were computed with a microcanonical ensemble for at least 1.5 ps. For a subset of 35 trajectories, the simulation time was continued to 3 ps. Thymine structures were analyzed in terms of the Cremer−Pople parameters[47] using the Boeyen's conformer classification scheme.[48]

Additional static calculations have been performed with the multireference configuration interaction method including single (MR-CIS) and single and double (MR-CISD) excitations, with the complete active space self-consistent-field second-order perturbation theory in its multistate version (MS-CASPT2)[49] and with the resolution-of-identity approximate coupled cluster to the second-order method (RI-CC2)[50–52] method. The MR-CISD and MR-CIS calculations were performed with a reference space containing six electrons in five orbitals using the orbitals computed at the CASSCF(10,8)/6-31G* level. We obtained this reference space from the CAS(10,8) space by applying a selection scheme based on natural-orbital occupation numbers where orbitals with an occupation larger than 0.9 and smaller than 0.1 were moved to doubly occupied and virtual space, respectively. Higher-order excitation effects were computed by the Davidson correction[35,53,54] for single-point calculations at the MR-CISD level. For the MS-CASPT2 calculations, we used the same CAS(10,8) space as that before by applying an IPEA shift[55] of 0.25 unless indicated differently. The 6-311G** and the 6-31G* basis sets were used.[33] The RI-CC2 calculations were performed with the TZVPP basis sets.[56]

The MRCI calculation were performed with the COLUMBUS program system.[57–59] For the dynamics simulations, the NEWTON-X program was used.[46,60] RI-CC2 calculations were performed with TURBOMOLE,[61] and MS-CASPT2 computations were performed with the MOLCAS program.[62] The Cremer-Pople parameters were obtained with help of the PLATON program.[63]

3. Results and Discussion

3.1. Potential Energy Surface of Thymine. The low-energy UV spectrum of thymine is characterized by a dark singlet S_1(nπ*) state closely followed by a bright S_2($\pi\pi$*) state.[14,32,64,65] Results obtained in this work are collected in Table 1. The vertical excitation energy into the nπ* state computed with different methods and basis sets agrees within a range of 0.4 eV. The increase in the basis set from double- to triple-ζ quality reduces the excitation energy by <0.2 eV. The effect of the IPEA shift in the MS-CASPT2 calculations is not pronounced for this particular state. As expected, the excitation into the $\pi\pi$* state is much more sensitive to the method. RI-CC2 excitation energies are reduced by 0.28 eV when the basis set is increased. At the MS-CASPT2 level, this stabilization amounts to only 0.14 eV. The inclusion of the IPEA shift in the MS-CASPT2 calculations increases the $\pi\pi$* excitation energy by almost 0.4 eV. The MR-CISD+Q excitation energy exceeds the MS-CASPT2 and RI-CC2 results by ~0.3 eV. At the CASSCF level used in the dynamics, the $\pi\pi$* state is found to be too high by about 1.5 to 2 eV. This is a well-known effect of the method[66,67] whose origin is connected to the lack of dynamical electron correlation and of diffuse basis functions. As will be discussed below, other topographic features of the potential energy surfaces computed at CASSCF level are in good agreement with results obtained at higher theoretical levels.

The minimum in the S_1 nπ* state optimized at the CASSCF level (Table 1 and Figure 1) shows a planar geometry with an elongation of the C_4-O_8 and C_5-C_6 bonds and shortening of the C_4-C_5 bond in comparison with the ground-state minimum geometry. Cartesian coordinates for this and all other structures discussed in this work are given in the Supporting Information. The S_2 state (Table 1 and Figure 1) is of $\pi_O\pi$* character and possesses a minimum with similar elongation of the C_4-O_8 and

TABLE 1: Vertical Excitation Energies, Energies of the S_1 and S_2 Minima and Energy of the Lowest MXS for Thymine Obtained with Several Methods

		energy (eV)					
geometry	state	CASSCF[a]	CC2	PT2/6-31G*[b]	PT2/6-311G**[c]	MR-CISD[d]	exptl
min S_0	S_0 cs	0.00	0.00[e] (0.00[f])	0.00 (0.00)	0.00 (0.00)	0.00	
	S_1 nπ*	5.31	5.06 (4.87)	5.29 (5.07[g])	5.23 (5.00[g])	5.31	
	S_2 $\pi\pi$*	7.12	5.56 (5.28)	5.58 (5.22[g])	5.44 (5.06[g])	5.72	4.95[h]
min S_1	S_0 cs	1.18	1.55 (1.48)	0.91	0.97	1.08	
	S_1 nπ*	3.98	4.04 (3.83)	4.38	4.41	4.58	
	S_2 $\pi\pi$*	6.18	5.45 (5.09)	5.99	5.99	6.03	
min S_2	S_0 cs	2.46		2.38	1.62	1.69	
	S_1 nπ*	4.18		4.84	4.64	4.80	
	S_2 $\pi_O\pi$*	5.94		5.65	5.70	5.68	
MXS ^{3,6}B	S_0 cs	2.87	2.50 (2.42)	2.38	2.34	2.52	
	S_1/S_2 $\pi\pi$*/nπ*	5.74	5.01 (4.85)	~5.3	~5.2	5.31	

[a] SA-3-CASSCF(10,8)/6-31G* (E_{ref} = −451.570922 au). [b] MS-CASPT2/SA-3-CAS(10,8)/6-31G* using CASSCF geometries (E_{ref} = −452.796617 au). [c] MS-CASPT2/SA-3-CAS(10,8)/6-311G** using CASSCF geometries (E_{ref} = −453.361535 au). [d] MR-CISD(6,5)+Q/SA-3-CASSCF(10,8)/6-31G* (E_{ref} = −452.465191 au). [e] RI-CC2/SV(P) using geometries optimized at the same level (E_{ref} = −452.461366 au). [f] RI-CC2/TZVPP using geometries optimized at the same level (E_{ref} = −453.361535 au). [g] Values obtained with IPEA = 0. [h] Ref 64.

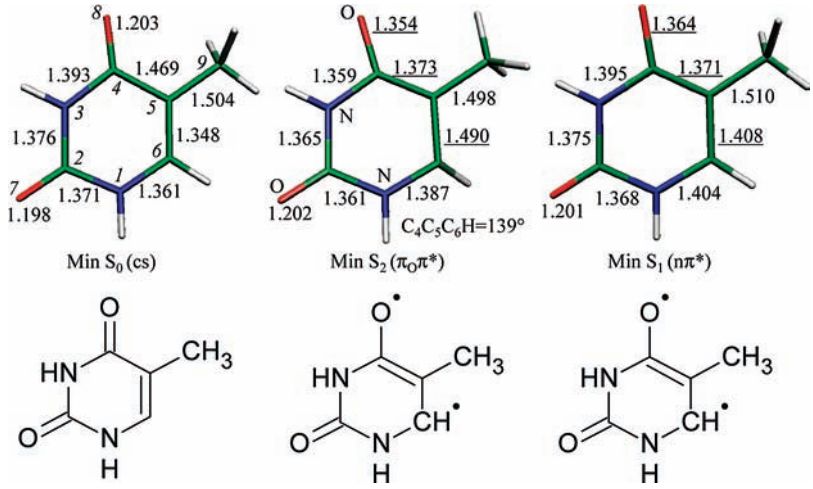

Figure 1. Ground- and excited-state minima of thymine and valence bond structures based on bond distances. Bond distances are given in angstroms, and main changes are underlined.

C_5-C_6 bonds and shortening of the C_4-C_5 bond. Different from the S_1 minimum, the S_2 minimum is pyramidalized at C_6. The existence of this minimum has been previously reported on the basis of the CASPT2 single-point and geometry optimizations.[29,68] This finding has been confirmed by optimization at the MR-CISD/6-31G* level performed in this work. The MR-CISD geometry is very similar to the CASSCF geometry. The root-mean-square deviation of the bond distances is smaller than 0.004 Å, and the maximum deviation occurs for the C_4C_5 bond distance, which is 0.02 Å shorter at CASSCF than at MR-CISD. No S_2 minimum could be located at the RI-CC2 level.

Starting at the ground-state geometry, the $\pi\pi$* state is connected through a barrierless path to a conical intersection with the ground state,[13,32] creating a direct diabatic pathway for internal conversion. Along the stabilization of the $\pi\pi$* state, it crosses the nπ* state. The nature of this crossing will be discussed in detail below. For now, it is important to bear in mind that when the crossing occurs there are two relaxation possibilities on the S_1 surface: either continuation with $\pi\pi$* character or change to nπ* character. In the nπ* state, two kinds of pathways for internal conversion exist: connecting the nπ* minimum to either the nπ*/S_0 or the $\pi\pi$*/S_0 conical intersections.[14] In the first case, the path shows an uphill profile, whereas in the second case, a barrier needs to be overcome.

The crossing between the S_2 and S_1 states occurs predominately at geometries puckered at the C_6 atom. We have identified six different minima on the S_2/S_1 intersection seam (MXS). Their energies are collected in Table 2, and their geometric structures are shown in Figure 3. Bond distances and Cremer−Pople parameters are given in Figure S3 and Table S1 of the Supporting Information. With the exception of the planar MXS, which corresponds to a $\sigma\pi$*/$\pi\pi$* crossing (σ orbital along the N_3C_4 bond), all other MXSs correspond to $\pi\pi$*/nπ* crossings.

TABLE 2: Energies of the MXSs for Thymine Relative to the Ground-State Energy Minimum Obtained at the SA-3-CASSCF(10,8)/6-31G* Level

MXS[a]	state	energy (eV)
^{3,6}B	S_0	2.87
	S_1/S_2	5.74
^{6}E	S_0	4.09
	S_1/S_2	6.83
planar	S_0	2.85
	S_1/S_2	6.84
E_5	S_0	5.77
	S_1/S_2	6.91
$^{3}T_1$	S_0	4.41
	S_1/S_2	6.14
$^{6}S_5$	S_0	3.77
	S_1/S_2	6.30

[a] B: boat; T: twisted boat; S: screw boat; E: envelope. The superscript and subscript indicate the atoms puckered above and below the ring plane, respectively.

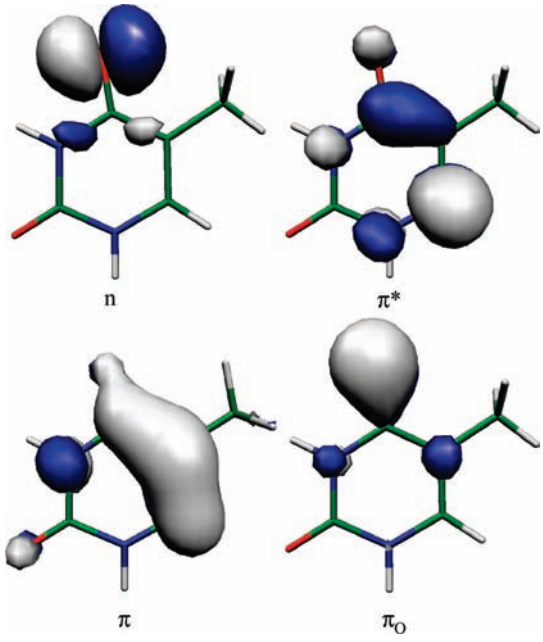

Figure 2. Molecular orbitals involved in the $\pi\pi^*$, $n\pi^*$, and $\pi_O\pi^*$ excitations.

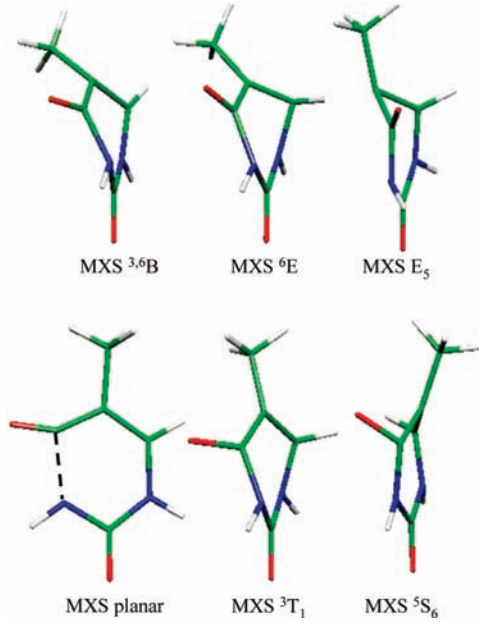

Figure 3. Geometries of the S_2/S_1 MXSs.

The lowest MXS (see Table 2), which has also been characterized by Hudock et al.,[29] shows a boat conformation puckered at atoms N_3 and C_6 (^{3,6}B). The **g** and **h** vectors defining the branching space[69] are shown in Figure S4 of the Supporting Information. Note that the contribution of out-of-plane directions is rather small.

The energy of the ^{3,6}B MXS is also given at RI-CC2, MS-CASPT2, and MR-CISD levels in Table 1. For the RI-CC2 calculation, the geometry optimization of the S_2 state led to S_2/S_1 state degeneracy. For the MS-CASPT2 method, the CASSCF geometry was used, which resulted in an energy split of 0.8 eV between states S_2 and S_1. The MXS entries in Table 1 for MS-CASPT2 correspond to the average between the two energy values. For the MR-CISD calculation, the MXS was optimized at this level starting from the CASSCF geometry. In all of these cases, the ^{3,6}B MXS is energetically accessible after vertical

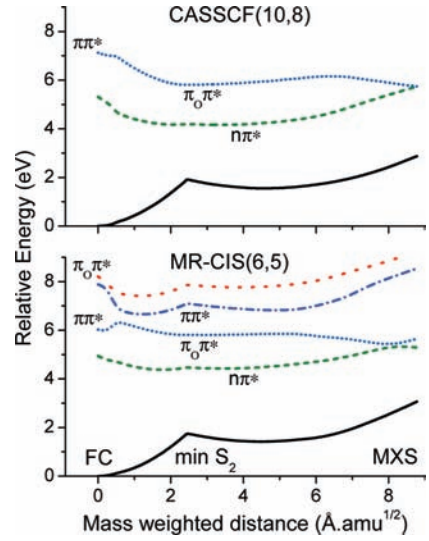

Figure 4. Potential energy curves along the linear interpolation paths between the Franck−Condon (FC) region and the S_2 minimum and from there to the S_2/S_1 ^{3,6}B MXS. The energies are computed at CASSCF(10,8)/6-31G* (top) and MR-CIS(6,5)/CASSCF(10,8)/6-31G* (bottom) levels.

excitation into the $\pi\pi^*$ state. Hudock et al.[29] have also shown that the pathway connecting the S_2 state minimum to this S_2/S_1 has the same features at both the CASSCF and MS-CASPT2 levels, which is confirmed at the MR-CISD level, as shown by the MR-CISD energies in Table 1. This agreement between CASSCF calculations and highly correlated methods is an important factor for the validation of the former method for dynamics simulations.

The other S_2/S_1 MXSs reported in this work have relatively high energy compared with the ^{3,6}B MXS (Table 2). Because of this, it is expected that they should play a significant role only when starting at the second $\pi\pi^*$ state, which is located at about 6.2 eV.[64] With the exception of the planar S_2/S_1 MXS, all others are conformational neighbors occurring in a restricted region of the $\theta-\phi$ space, with $90 < \theta < 120°$ and $60 < \phi < 150°$ (and the symmetrical counterpart, $60 < \theta < 90°$ and $240 < \phi < 330°$). This is an indication that all of these minima belong to the same branch of crossing seam, which should span the E_5, $^6S_5$, ^{6}E, ^{3,6}B, and $^3T_1$ conformations sequentially.

Besides the planarity, the main feature of the planar MXS is the ring-opening character at the C_3-C_4 bond. (See Figure 3.) This kind of conical intersection has been recently reported for a number of heterocycles[70–73] and has been observed to take place in high-energy deactivation processes in adenine.[28]

Throughout this section, a comparison of energies and geometric features of stationary points and MXSs of thymine using different methods has been presented. This comparison as well as the results reported in ref 29 clearly show that apart from the high vertical excitation of the $\pi\pi^*$ state, all other topographic features computed at the CASSCF level are in good agreement with results obtained with MR-CISD and MS-CASPT2 methods. Additionally, the potential energy curves along the linearly interpolated path between the Franck−Condon region and the S_2 minimum and from this minimum on to the S_2/S_1 ^{3,6}B MXS are shown in Figure 4. The main features of these paths computed at CASSCF level (top) are well reproduced when the same paths are computed at the MR-CIS(6,5)/SA-3-CASSCF(10,8)/6-31G* level (bottom) using the same geometries. Five states were computed in the MR-CIS calculations, which allows us to unveil the avoided crossings giving rise to

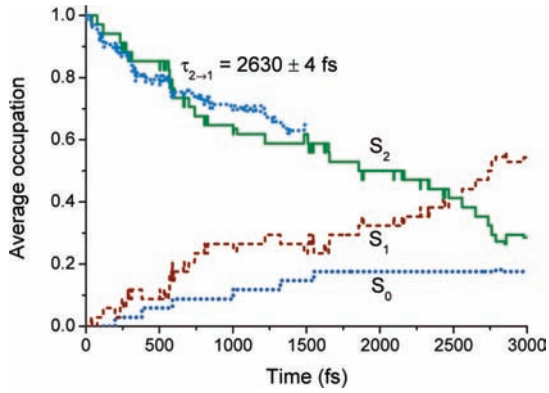

Figure 5. Time evolution of the average occupation of the adiabatic states.

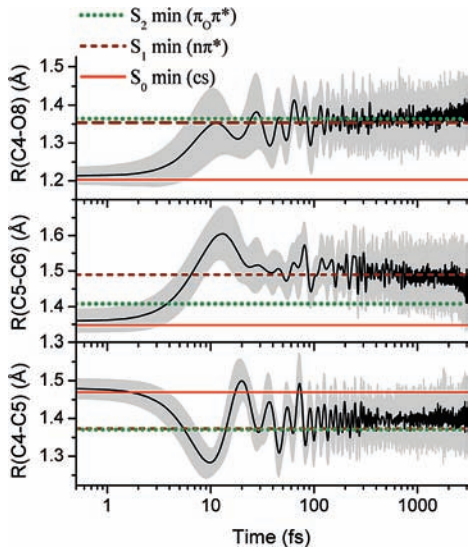

Figure 6. C_4-O_8, C_5-C_6, and C_4-C_5 bond distances as a function of time averaged over all trajectories. The gray area corresponds to plus/minus one standard deviation around the average.

the $\pi\pi^*/\pi_O\pi^*$ exchange of character of the S_2 state. Together, these facts indicate that the CASSCF method can adequately describe qualitative features of the excited state dynamics of thymine.

3.2. Dynamics Results. The time evolution of the fraction of trajectories in each state is shown in Figure 5 for the subset of 35 trajectories running for 3 ps. The occupation of the S_2 state decreases slowly, showing a time constant of 2.6 ps. The ground state does not show any appreciable population in the first 3 ps. This situation agrees well with the observations obtained from the multiple spawning simulations performed by Hudock et al.[29] The dotted line close to the S_2 occupation is the same quantity computed with the complete set of 70 trajectories propagated for 1.5 ps. In this case, the time constant is slightly longer, 2.8 ps.

As discussed above, the main geometrical distortions from the ground-state minimum to the S_2 minimum were found in the elongation of the C_5-C_6 and C_4-O_8 bonds and in the shrinking of the C_4-C_5 bond. The same geometrical patterns are observed in the dynamics. (See Figure 6.) Starting from a Wigner distribution centered at the ground-state geometry, the average values of these three quantities change to those close to the S_2 minimum values in about 100 fs or less. Coherent oscillations of the C_4-O_8 and C_4-C_5 bond distances are observed within this time. From 100 fs to 2 ps, the bond distances oscillate around the S_2 minimum values. After 2 ps,

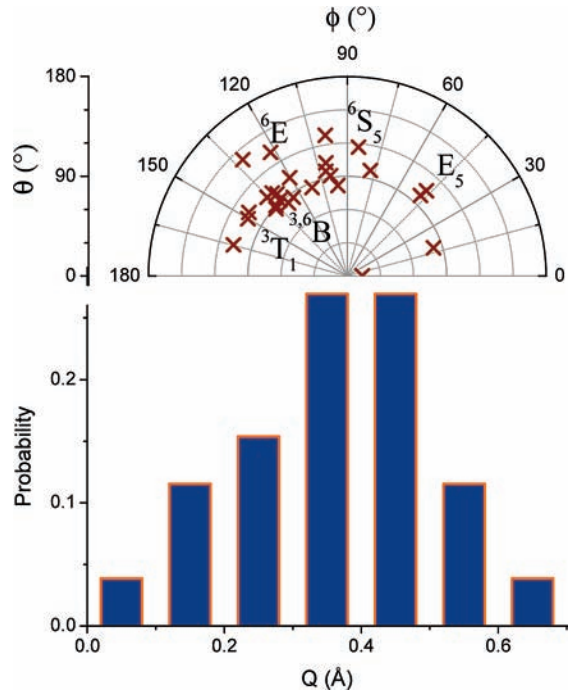

Figure 7. Cremer−Pople parameters of thymine structures at the hopping time. In the upper panel, the distribution in the $\theta-\phi$ space is shown, whereas the Q values histogram is plotted in the bottom panel.

the average value starts to deviate in the direction of the S_1 minimum value, indicating the increase in S_1 population. This effect is particularly pronounced in the C_5-C_6 bond distance.

The $S_2 \rightarrow S_1$ hoppings take place at moderately puckered geometries. The average degree of puckering at the hopping time is $\langle Q \rangle = 0.36 \pm 0.14$ Å (bottom panel of Figure 7), whereas at the same time, the energy gap shows an exponential decay whose average is 0.32 eV. The ^{3,6}B conformation is the most frequent structure observed at the hoppings, although $^3T_1$, ^{6}E, $^6S_5$, and E_5 conformations have been observed as well (Figure 7, upper panel). S_2/S_1 MXSs have been optimized for all of these conformations, as discussed above (Figure 3). The preference for the ^{3,6}B conformation is consistent with the lower energy of this section of the crossing seam in comparison with the energies of other MXSs (Table 2).

The analysis of one typical trajectory helps us to understand details of how the $S_2 \rightarrow S_1$ deactivation occurs. For this particular trajectory, Figure 8 shows that until 1820 fs, a relatively large S_2-S_1 energy gap (~1.6 eV) is maintained. Almost suddenly, between 1820 and 1830 fs, this gap is reduced to a few tenths of an electronvolt (~0.4 eV, Figure 8, top left) when the character of the S_2 state changes from $\pi_O\pi^*$ to $\pi\pi^*$. (See the orbitals in Figure 2.) It is important to note that the gap is mainly reduced by destabilization of the S_1 ($n\pi^*$) state and not by stabilization of the S_2 state. Even though thymine has shown a high degree of puckering even before this gap reduction (Figure 8, top right), it is the shrinking of the C_4-O_8 bond (not shown) in the ^{6}E and ^{3,6}B conformations at about 1830 fs (bottom right) that promotes the crossing. This is consistent with the small contribution of out-of-plane modes to the branching space mentioned in the previous section. The crossing itself occurs via a strong mixing of the $n\pi^*$ and $\pi\pi^*$ configurations (bottom left). After hopping to the S_1 state, the mixing quickly decreases, and the S_1 state reacquires the $n\pi^*$ character.

The same general picture is observed when the whole set of trajectories is analyzed. Statistics over all trajectories show the

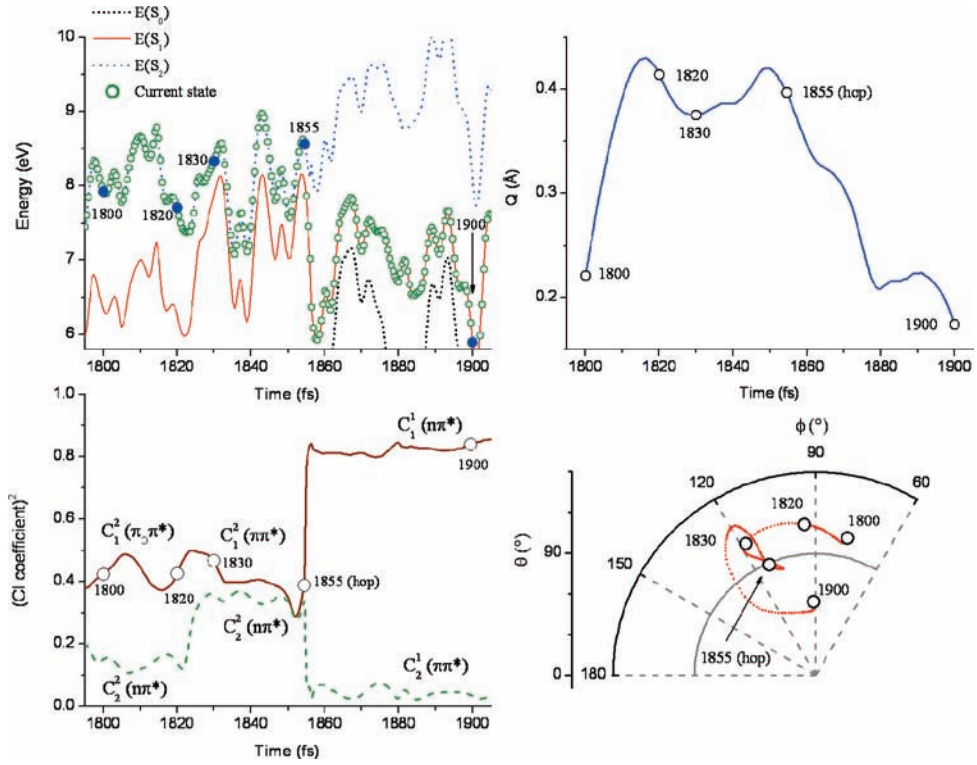

Figure 8. Analysis of a single trajectory. Top-left: Potential energies of the S_2, S_1, and S_0 states during the dynamics. The circles indicate the current state in each time step. Top-right: time evolution of the Cremer−Pople parameter Q. Bottom-left: Time evolution of the squares of the two main CI coefficients C_i^k (i = 1,2) for the current state k. Bottom-right: Time evolution of the Cremer−Pople parameters θ (radial coordinate) and ϕ (polar coordinate).

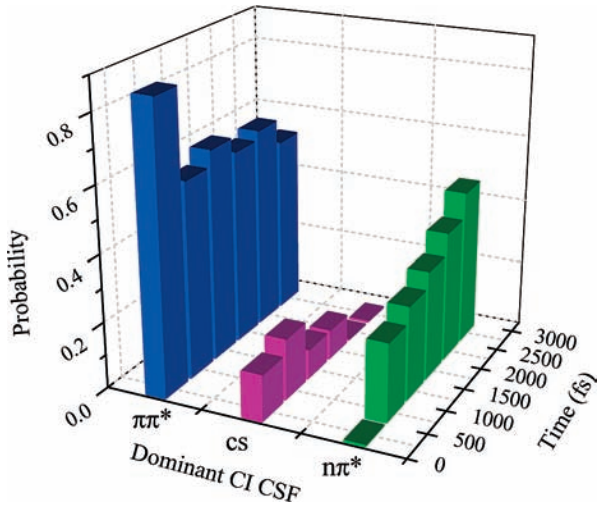

Figure 9. Distribution of the dominant CI configuration state function (CSF) in the electronic wave function of the current state as a function of time. $\pi\pi^*$ columns also include $\pi_O\pi^*$ contributions.

wave function of the state in which the system currently is in during the first picosecond consists of a mixing of $\pi\pi^*$ (dominant) and closed shell, cs, configurations. (See Figure 9.) At about 1 ps, the contribution of the $n\pi^*$ configuration starts to increase, reflecting the increasing population of the S_1 state. Between 2.5 and 3.0 ps, the populations of the $\pi\pi^*$ and $n\pi^*$ states are roughly the same. Note that in Figure 9, the $\pi\pi^*$ and $\pi_O\pi^*$ contributions are shown together. Because the cs configuration has a larger contribution to the wave function in the $\pi\pi^*$ region of the S_2 state than in the $\pi_O\pi^*$ region, the occurrence of the cs contributions is an indication that the $\pi\pi^*$ region is often visited during the dynamics.

As also mentioned above, the existence of this minimum cannot be confirmed at the RI-CC2 level. Its absence accelerates the dynamics simulations at this level to a point that the decay to S_1 state is estimated to take place in less than 100 fs. This result is similar to that obtained at the OM2 semiempirical level[26] mentioned in the Introduction, which showed $S_2 \rightarrow S_1$ deactivation occurring in only 17 fs. However, the clear existence of the $\pi_O\pi^*$ minimum at both CASPT2[29,68] and MR-CI levels is a strong indication that RI-CC2 and OM2 methods are predicting the wrong dynamics for thymine.

3.3. Photophysics of Thymine. According to the present results, the dynamics of thymine proceeds in the following way. (See Figure 10.) After the photoexcitation into the S_2 $\pi\pi^*$ state, thymine relaxes adiabatically into the $\pi_O\pi^*$ state. This process occurs in less than 100 fs and is characterized by planar relaxation of the ring with C_5-C_6 and C_4-O_8 stretching and C_4-C_5 shrinking, corresponding to the formation of a biradicaloid structure with radical centers at the O_8 and C_6 atoms. In the next 2.5 ps, thymine remains on the S_2 surface, mostly keeping the $\pi_O\pi^*$ character but also moving into regions of $\pi\pi^*$ character for short periods of time (<50 fs). Eventually, thymine reaches the intersection seam between the S_2 and S_1 states. Geometrically, this mainly happens at conformations showing a moderate degree of puckering at atom C_6 and shortening of the C_4-O_8 bond, especially in the boat $^{3,6}B$ conformation, which corresponds to the lowest region of the intersection seam. In the S_1 state, thymine remains in regions of $n\pi^*$ character, moving into the $\pi\pi^*$ region for short periods of time varying from 20 to 60 fs.

As discussed in the Introduction, UV-excited thymine has a lifetime that is a few times longer than those of the other nucleobases, and three main hypotheses have been proposed to explain this feature. The deactivation mechanism discussed in

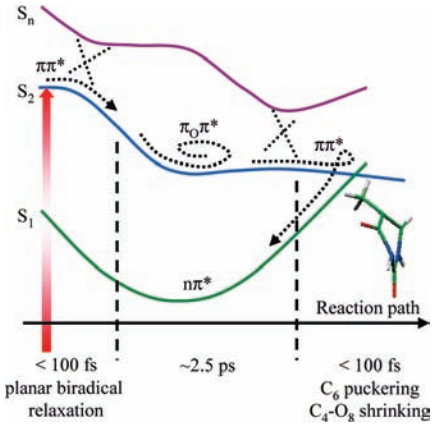

Figure 10. Scheme of the dynamics of thymine in the S_2 state until the deactivation to the S_1 state. The ground state is not shown. Note that the times summing up to ~2.6 ps correspond to the time to populate the S_1 state and should not be taken as an estimate for the total excited state lifetime.

the previous paragraph corroborates the hypothesis raised in ref 29, which indicates that the trapping in the S_2 state is the main reason for the long lifetime. Moreover, the propagation of the dynamics for much longer times than those in ref 29 allows us to refine this explanation by exploring the mechanistic and wave function features of the S_2/S_1 deactivation process.

The present simulations have shown that a change of the character of the S_2 state occurs, which seems to be crucial for keeping thymine far from the S_2/S_1 crossing region. This implies that a complete description of the thymine dynamics involves a third excited state (S_3), as shown in Figure 4 (bottom) and indicated schematically in Figure 10. When thymine finally moves into the $\pi\pi^*$ region of the S_2 state, the crossing seam is reached mainly by destabilization of the S_1 state rather than stabilization of S_2. This can be inferred from the static calculations as well: the data in Tables 1 and 2 show that the energy of the S_2 minimum is only 0.2 eV higher than the energy of the lowest conical intersection. From a mechanistic point of view, this is a relevant distinction. If the stabilization of S_2 was the reason for the crossing, thymine could slide down toward the crossing in any of the several instances that the S_2 state character changes from $\pi_O\pi^*$ to $\pi\pi^*$. The result would be a shorter lifetime of the S_2 state. Because of the flatness of the S_2 potential energy surface, the crossing is reached only when the correct combination of coordinates is statistically tuned. This effect, rather than the presence of a barrier to be overcome, seems to be the main reason for the long amount of time spent in the S_2 state.

Although we are confident that the 2.6 ps average time obtained for the $S_2 \rightarrow S_1$ deactivation is a main reason for the long lifetime of thymine, it should be observed that this value is still considerably shorter than the 5 to 6 ps lifetime experimentally measured.[1,2,4] This difference can be jointly attributed to a few different factors. First and most importantly, the simulations show that thymine relaxes to the $n\pi^*$ region of the S_1 state. As discussed in refs 13 and 14, this means that the S_1/S_0 crossing seam should be reached by either overcoming barriers or moving uphill in sloped intersections. This implies that the $S_1 \rightarrow S_0$ deactivation may also take a relatively long time, adding to the $S_2 \rightarrow S_1$ deactivation time to compose the global lifetime. Other important factors that should also contribute to accelerating the $S_2 \rightarrow S_1$ deactivation process are the high CASSCF vertical excitation energy of S_2 and the initial conditions, which in our simulations are taken from the whole absorption spectrum, including regions of higher energies than those used for the pump pulse.

Seven trajectories relaxed to the ground state within the 3 ps simulation time. Even though this set is certainly not statistically representative, it is interesting to note two facts. First, the trajectories in the S_1 state seem to be evenly split between those hopping at the $\pi\pi^*$/cs and those hopping at the $n\pi^*$/cs regions of the crossing seam. Second, despite the fact that a few trajectories directly follow the $\pi\pi^*$ pathway from the S_2 to the S_1 state, with the exception of one case, they did not continue directly toward the $\pi\pi^*$/cs conical intersection with the ground state, as proposed in ref 32. Instead, they turned to the $n\pi^*$ region of S_1 and subsequently followed a dynamics similar to that of the other trajectories.

4. Conclusions

Nonadiabatic dynamics simulations have been performed at ab initio CASSCF level for thymine to investigate the $S_2 \rightarrow S_1$ deactivation process. Seventy trajectories were propagated for a minimum of 1.5 ps, and 35 trajectories were propagated for 3 ps. We have checked the quality of the CASSCF potential energy surfaces by supporting MR-CIS, MR-CISD, MS-CASPT2, and RI-CC2 calculations.

Thymine has the longest lifetime among the five naturally occurring nucleobases, and three different hypotheses have been proposed to explain this feature: trapping in the S_2 $\pi\pi^*$ minimum,[29] trapping in the S_1 $n\pi^*$ minimum,[13] and trapping in the S_1 $\pi\pi^*$ minimum.[32] It is important to note that in all of these investigations, very similar, flat energy paths leading from the Franck−Condon region to the S_2/S_1 conical intersection were found. This example clearly demonstrates again the importance of dynamics simulations for the assessment of the time scales of individual mechanistic steps. The simulation times used in the present work could be extended long enough to account fully for the deactivation from S_2 to S_1 and even to find indications for the transfer from S_1 to S_0. The results obtained fully corroborate the first hypothesis and show in detail how the process takes place.

The trapping in the S_2 state occurs at a $\pi_O\pi^*$ region of the potential energy surface with short incursions into the $\pi\pi^*$ region. The occurrence of the $\pi_O\pi^*$ S_2 minimum, whose existence has been checked at the MR-CISD level, is due to avoided crossings with higher states (S_3 and S_4) along the main reaction path. Because of the flatness of the surface, the crossing with the S_1 state is delayed and statistically reached when thymine assumes geometric configurations that destabilize the S_1 state. The $S_2 \rightarrow S_1$ deactivation occurs in 2.6 ps mainly at boat ^{3,6}B conformations, corresponding to the lowest region of the S_2/S_1 crossing seam. This process is schematically illustrated in Figure 10.

The S_1 state dynamics mainly happens in the $n\pi^*$ region, although the $\pi\pi^*$ character occurs for short periods smaller than 60 fs. The 3 ps simulation time was not sufficient to investigate the $S_1 \rightarrow S_0$ deactivation process with adequate statistical significance. This fact shows that not only the $\pi_O\pi^*$ S_2 trapping but also the trapping in the $n\pi^*$ S_1 minimum contributes to the elongation of the excited-state lifetime of thymine.

Acknowledgment. We thank L. Blancafort for useful discussions and acknowledge the technical support and computer time at the Linux PC cluster Schrödinger III of the computer center of the University of Vienna and the Poznan Supercomputing and Networking Center. This work has been supported by the Austrian Science Fund within the framework of the

Special Research Program F16 (Advanced Light Sources) and project P18411−N19 by the Partnership in International Research and Education (PIRE) program of the American National Science Foundation under no. OISE-0730114. Support by the grant from the Ministry of Education of the Czech Republic (Center for Biomolecules and Complex Molecular Systems, LC512) and by the Praemium Academiae of the Academy of Sciences of the Czech Republic, awarded to Pavel Hobza in 2007, is gratefully acknowledged. This work was part of the research project Z40550506 of the Institute of Organic Chemistry and Biochemistry of the Academy of Sciences of the Czech Republic.

Supporting Information Available: Orbitals, absorption spectrum, Cartesian coordinates, and additional geometric characterization. This material is available free of charge via the Internet at http://pubs.acs.org.

References and Notes

(1) Canuel, C.; Mons, M.; Piuzzi, F.; Tardivel, B.; Dimicoli, I.; Elhanine, M. *J. Chem. Phys.* **2005**, *122*, 074316.
(2) Kang, H.; Lee, K. T.; Jung, B.; Ko, Y. J.; Kim, S. K. *J. Am. Chem. Soc.* **2002**, *124*, 12958.
(3) Crespo-Hernández, C. E.; Cohen, B.; Hare, P. M.; Kohler, B. *Chem. Rev.* **2004**, *104*, 1977.
(4) Ullrich, S.; Schultz, T.; Zgierski, M. Z.; Stolow, A. *Phys. Chem. Chem. Phys.* **2004**, *6*, 2796.
(5) Saigusa, H. *J. Photochem. and Photobiol., C* **2006**, *7*, 197.
(6) Blancafort, L. *J. Am. Chem. Soc.* **2006**, *128*, 210.
(7) Chen, H.; Li, S. H. *J. Phys. Chem. A* **2005**, *109*, 8443.
(8) Chung, W. C.; Lan, Z. G.; Ohtsuki, Y.; Shimakura, N.; Domcke, W.; Fujimura, Y. *Phys. Chem. Chem. Phys.* **2007**, *9*, 2075.
(9) Marian, C. M. *J. Chem. Phys.* **2005**, *122*, 104314.
(10) Perun, S.; Sobolewski, A. L.; Domcke, W. *J. Am. Chem. Soc.* **2005**, *127*, 6257.
(11) Serrano-Andrés, L.; Merchán, M.; Borin, A. C. *Proc. Natl. Acad. Sci. U.S.A.* **2006**, *103*, 8691.
(12) Gustavsson, T.; Banyasz, A.; Lazzarotto, E.; Markovitsi, D.; Scalmani, G.; Frisch, M. J.; Barone, V.; Improta, R. *J. Am. Chem. Soc.* **2006**, *128*, 607.
(13) Perun, S.; Sobolewski, A. L.; Domcke, W. *J. Phys. Chem. A* **2006**, *110*, 13238.
(14) Zechmann, G.; Barbatti, M. *J. Phys. Chem. A* **2008**, *112*, 8273.
(15) Zgierski, M. Z.; Patchkovskii, S.; Fujiwara, T.; Lim, E. C. *J. Phys. Chem. A* **2005**, *109*, 9384.
(16) Ismail, N.; Blancafort, L.; Olivucci, M.; Kohler, B.; Robb, M. A. *J. Am. Chem. Soc.* **2002**, *124*, 6818.
(17) Matsika, S. *J. Phys. Chem. A* **2004**, *108*, 7584.
(18) Marian, C. M. *J. Phys. Chem. A* **2007**, *111*, 1545.
(19) Perun, S.; Sobolewski, A. L.; Domcke, W. *Mol. Phys.* **2006**, *104*, 1113.
(20) Blancafort, L.; Cohen, B.; Hare, P. M.; Kohler, B.; Robb, M. A. *J. Phys. Chem. A* **2005**, *109*, 4431.
(21) Nielsen, S. B.; Solling, T. I. *ChemPhysChem* **2005**, *6*, 1276.
(22) Barbatti, M.; Lischka, H. *J. Phys. Chem. A* **2007**, *111*, 2852.
(23) Frey, J. A.; Leist, R.; Tanner, C.; Frey, H. M.; Leutwyler, S. *J. Chem. Phys.* **2006**, *125*, 114308.
(24) Fabiano, E.; Thiel, W. *J. Phys. Chem. A* **2008**, *112*, 6859.
(25) Lei, Y.; Yuan, S.; Dou, Y.; Wang, Y.; Wen, Z. *J. Phys. Chem. A* **2008**, *112*, 8497.
(26) Lan, Z.; Fabiano, E.; Thiel, W. *J. Phys. Chem. B* **2009**, *113*, 3548.
(27) Langer, H.; Doltsinis, N. L.; Marx, D. *ChemPhysChem* **2005**, *6*, 1734.
(28) Barbatti, M.; Lischka, H. *J. Am. Chem. Soc.* **2008**, *130*, 6831.
(29) Hudock, H. R.; Levine, B. G.; Thompson, A. L.; Satzger, H.; Townsend, D.; Gador, N.; Ullrich, S.; Stolow, A.; Martinez, T. J. *J. Phys. Chem. A* **2007**, *111*, 8500.
(30) Hudock, H. R.; Martinez, T. J. *ChemPhysChem* **2008**, *9*, 2486.
(31) Groenhof, G.; Schafer, L. V.; Boggio-Pasqua, M.; Goette, M.; Grubmuller, H.; Robb, M. A. *J. Am. Chem. Soc.* **2007**, *129*, 6812.
(32) Merchan, M.; Gonzalez-Luque, R.; Climent, T.; Serrano-Andres, L.; Rodriguez, E.; Reguero, M.; Pelaez, D. *J. Phys. Chem. B* **2006**, *110*, 26471.
(33) Hehre, W. J.; Ditchfield, R.; Pople, J. A. *J. Chem. Phys.* **1972**, *56*, 2257.
(34) Shepard, R.; Lischka, H.; Szalay, P. G.; Kovar, T.; Ernzerhof, M. *J. Chem. Phys.* **1992**, *96*, 2085.
(35) Shepard, R. The Analytic Gradient Method for Configuration Interaction Wave Functions. In *Modern Electronic Structure Theory*; Yarkony, D. R., Ed.; World Scientific: Singapore, 1995; Vol. 1, p 345.
(36) Lischka, H.; Dallos, M.; Shepard, R. *Mol. Phys.* **2002**, *100*, 1647.
(37) Dallos, M.; Lischka, H.; Shepard, R.; Yarkony, D. R.; Szalay, P. G. *J. Chem. Phys.* **2004**, *120*, 7330.
(38) Lischka, H.; Dallos, M.; Szalay, P. G.; Yarkony, D. R.; Shepard, R. *J. Chem. Phys.* **2004**, *120*, 7322.
(39) Tully, J. C. *Faraday Discuss.* **1998**, *110*, 407.
(40) Swope, W. C.; Andersen, H. C.; Berens, P. H.; Wilson, K. R. *J. Chem. Phys.* **1982**, *76*, 637.
(41) Butcher, J. *J. Assoc. Comput. Mach.* **1965**, *12*, 124.
(42) Pittner, J.; Lischka, H.; Barbatti, M. *Chem. Phys.* **2009**, *356*, 147.
(43) Granucci, G.; Persico, M. *J. Chem. Phys.* **2007**, *126*, 134114.
(44) Tully, J. C. *J. Chem. Phys.* **1990**, *93*, 1061.
(45) Hammes-Schiffer, S.; Tully, J. C. *J. Chem. Phys.* **1994**, *101*, 4657.
(46) Barbatti, M.; Granucci, G.; Persico, M.; Ruckenbauer, M.; Vazdar, M.; Eckert-Maksic, M.; Lischka, H. *J. Photochem. Photobiol., A* **2007**, *190*, 228.
(47) Cremer, D.; Pople, J. A. *J. Am. Chem. Soc.* **1975**, *97*, 1354.
(48) Boeyens, J. C. A. *J. Chem. Crystallogr.* **1978**, *8*, 317.
(49) Finley, J.; Malmqvist, P. A.; Roos, B. O.; Serrano-Andrés, L. *Chem. Phys. Lett.* **1998**, *288*, 299.
(50) Christiansen, O.; Koch, H.; Jorgensen, P. *Chem. Phys. Lett.* **1995**, *243*, 409.
(51) Hättig, C.; Weigend, F. *J. Chem. Phys.* **2000**, *113*, 5154.
(52) Hättig, C.; Köhn, A. *J. Chem. Phys.* **2002**, *117*, 6939.
(53) Langhoff, S. R.; Davidson, E. R. *Int. J. Quantum Chem.* **1974**, *8*, 61.
(54) Bruna, P. J.; Peyerimhoff, S. D.; Buenker, R. J. *Chem. Phys. Lett.* **1980**, *72*, 278.
(55) Ghigo, G.; Roos, B. O.; Malmqvist, P.-A. *Chem. Phys. Lett.* **2004**, *396*, 142.
(56) Schafer, A.; Horn, H.; Ahlrichs, R. *J. Chem. Phys.* **1992**, *97*, 2571.
(57) Lischka, H.; Shepard, R.; Brown, F. B.; Shavitt, I. *Int. J. Quantum Chem.* **1981**, *S15*, 91.
(58) Lischka, H.; Shepard, R.; Pitzer, R. M.; Shavitt, I.; Dallos, M.; Müller, T.; Szalay, P. G.; Seth, M.; Kedziora, G. S.; Yabushita, S.; Zhang, Z. Y. *Phys. Chem. Chem. Phys.* **2001**, *3*, 664.
(59) Lischka, H.; Shepard, R.; Shavitt, I.; Pitzer, R. M.; Dallos, M.; Mueller, T.; Szalay, P. G.; Brown, F. B.; Ahlrichs, R.; Boehm, H. J.; Chang, A.; Comeau, D. C.; Gdanitz, R.; Dachsel, H.; Ehrhardt, C.; Ernzerhof, M.; Hoechtl, P.; Irle, S.; Kedziora, G.; Kovar, T.; Parasuk, V.; Pepper, M. J. M.; Scharf, P.; Schiffer, H.; Schindler, M.; Schueler, M.; Seth, M.; Stahlberg, E. A.; Zhao, J.-G.; Yabushita, S.; Zhang, Z.; Barbatti, M.; Matsika, S.; Schuurmann, M.; Yarkony, D. R.; Brozell, S. R.; Beck, E. V.; Blaudeau, J.-P. *COLUMBUS, an Ab Initio Electronic Structure Program*, release 5.9.1 2006. www.univie.ac.at/columbus.
(60) Barbatti, M.; Granucci, G.; Ruckenbauer, M.; Pittner, J.; Persico, M.; Lischka, H. *NEWTON-X: a Package for Newtonian Dynamics Close to the Crossing Seam*, 2007. www.univie.ac.at/newtonx.
(61) Ahlrichs, R.; Bär, M.; Häser, M.; Horn, H.; Kölmel, C. *Chem. Phys. Lett.* **1989**, *162*, 165.
(62) Karlström, G.; Lindh, R.; Malmqvist, P. A.; Roos, B. O.; Ryde, U.; Veryazov, V.; Widmark, P. O.; Cossi, M.; Schimmelpfennig, B.; Neogrady, P.; Seijo, L. *Comput. Mater. Sci.* **2003**, *28*, 222.
(63) Spek, A. L. *J. Appl. Crystallogr.* **2003**, *36*, 7.
(64) Abouaf, R.; Pommier, J.; Dunet, H. *Chem. Phys. Lett.* **2003**, *381*, 486.
(65) Fleig, T.; Knecht, S.; Hättig, C. *J. Phys. Chem. A* **2007**, *111*, 5482.
(66) Müller, T.; Dallos, M.; Lischka, H. *J. Chem. Phys.* **1999**, *110*, 7176.
(67) Frutos, L. M.; Andruniow, T.; Santoro, F.; Ferre, N.; Olivucci, M. *Proc. Natl. Acad. Sci. U.S.A.* **2007**, *104*, 7764.
(68) Gonzalez, L.; Gonzalez-Vazquez, J.; Samoylova, E.; Schultz, T. *AIP Conf. Proc.* **2008**, *1080*, 169.
(69) Yarkony, D. R. *Conical Intersections: Electronic Structure, Dynamics & Spectroscopy*; World Scientific Publishing Company, 2004.
(70) Perun, S.; Sobolewski, A. L.; Domcke, W. *Chem. Phys.* **2005**, *313*, 107.
(71) Gavrilov, N.; Salzmann, S.; Marian, C. M. *Chem. Phys.* **2008**, *349*, 269.
(72) Salzmann, S.; Kleinschmidt, M.; Tatchen, J.; Weinkauf, R.; Marian, C. M. *Phys. Chem. Chem. Phys.* **2008**, *10*, 380.
(73) Vazdar, M.; Eckert-Maksic, M.; Barbatti, M.; Lischka, H. *Mol. Phys.* **2009**, *107*, 845.

JP905085X